ANL/XFD/CP--87518
CONF-9510119--14

PERFORMANCE OF CRYOGENICALLY COOLED, HIGH-HEAT-LOAD SILICON CRYSTAL MONOCHROMATORS WITH POROUS MEDIA AUGMENTATION*

C. S. Rogers, D. M. Mills, L. Assoufid, and T. Graber
Experimental Facilities Division, Advanced Photon Source,
Argonne National Laboratory, Argonne, IL 60439

January 1996

Presented at the SRI '95 APS X-ray Centennial Symposium/Seventh Users Meeting for the APS, Argonne, IL, October 16-20, 1995; to be published in the proceedings as a peer-reviewed volume of the *Review of Scientific Instruments* in CD-ROM format.

*This work supported by the U.S. Department of Energy, Basic Energy Sciences-Materials Sciences, under contract #W-31-109-ENG-38.

improve the heat transfer coefficient while maintaining single-phase flow are being investigated. One of the simplest and most promising methods is to increase the turbulence and effectiveness of the heat exchanger by using porous media enhancement. This is a well-known technique for heat transfer augmentation in many applications and has been proposed for use in high-heat-flux optics by numerous authors.[9-15]

II. THE CRYSTALS AND CRYOGENIC COOLING SYSTEM

A photograph of the unenhanced crystal is shown in Fig. 1. Seven 6.4-mm-diameter coolant channels, spaced 9.5 mm center to center, were drilled into a rectangular block of (111)-oriented silicon. The dimensions of the crystal are 86 x 60 x 25 mm^3. The diffracting surface of the Si was 12 mm from the top of channels. Two such crystals were fabricated. In one, the coolant channels were left as drilled, and, in the second, a Cu mesh insert was bonded into the coolant channels using a thermally conductive paste.[16] The insert was made by rolling and compressing an interlaced Cu screen. Copper mesh was chosen because of it high thermal conductivity, ease of fabrication, and its conformability; the Cu mesh is very "springy", which means that under stress it will tend to deform without imposing a large force on the much stiffer Si. The heat transfer enhancement arises from the fin effect of the wire mesh and turbulent mixing of the fluid. Experiments have shown that the heat transfer coefficient can be increased by a factor from about 4 to 10 over plain channels when water is used as the coolant.[17,18] Also, the onset of nucleate boiling (ONB) is delayed to much higher wall temperatures compared to a plain channel. This is very beneficial because, unlike plain channels, the mesh-enhanced channels cannot support much vapor generation due to rapid occlusion of the flow passage. Good thermal contact between the mesh and wall is necessary to achieve the maximum fin effect. It has been shown that the heat transfer coefficient increases by about a factor of 2 for water when the mesh is brazed into the channel as opposed to just a tight press fit due to the increased conduction into the wire mesh.

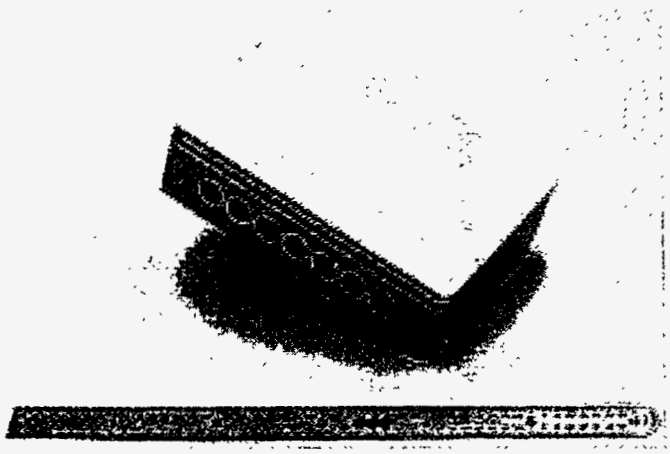

FIG. 1. Photograph of the unenhanced crystal. The enhanced crystal had porous Cu mesh inserts bonded into the 6.4-mm-diameter channels using a Ag-loaded glass frit[16], but otherwise was identical to the unenhanced crystal.

A closed-loop pumping system was used to supply pressurized liquid nitrogen at 78 K to the optic. An integral shell-and-tube heat exchanger was used to remove the heat from the optic-loop liquid by boiling liquid nitrogen at atmospheric pressure in the shell side. The cryogenic system has been thoroughly described elsewhere.[15] However, one important modification was made to the original design, the vane pump was replaced with a Barber-Nichols Inc. (Denver, CO, USA) centrifugal pump. It provides volume flow rates up to 20 l/min at a differential pressure of 50 psi.

III. MONOCHROMATOR PERFORMANCE

The cryogenically cooled optic was housed in a vacuum chamber located approximately 26.5 meters downstream from the CHESS 24-pole permanent-magnet wiggler, which has a critical energy, E_c, of 22 keV.[19] The ring energy was 5.26 GeV, and the deflection parameter, K, was 21.9. A total of 0.058 inches of Be (four vacuum windows) and 0.010 inches of graphite (Be window prefilter) was between the source and the test optic. Approximately half of the total horizontal extent of the wiggler beam is allotted to the F2 station. Given these parameters, the calculated incident power is 21.125 W/mA and the calculated horizontal beam width is about 58 mm at the crystal. The measured beam width and power were 40-45 mm and 14.2 W/mA. From observations of the intensity and shape of the beam, it was surmised that the most intense central portion of the beam was obstructed. All of the experiments described below were made with the vertical slits completely open. The calculated height of the beam at the crystal was: $(1.2/\gamma)$ x 26.5 m = 3.1 mm (FWHM) where $1/\gamma = 97$ μrad.

The power incident on the crystal was varied by adjusting the horizontal slits. In previous experiments on water and liquid Ga cooled (room temperature), two-piece bonded crystals, it was not practical to use this technique for altering the power because of significant spatial variations of mechanical strain resulting from the fabrication and mounting process.[20-22] This strain would often cause the width of the rocking curve to increase as a larger area of the crystal was illuminated, even for highly attenuated beams. A noteworthy difference between these cryogenic crystals and the previously tested room temperature crystals is that the improved thermal conductivity of Si at cryogenic temperatures permits a much thicker "hot face" (the distance between the diffraction surface and the coolant channels) facilitating the use of In O-rings, or C-rings rather than bonding processes to seal the coolant channels. This design change results in much lower mechanical strain so the beam footprint can cover the entire crystal face with minimal impact on the rocking curve width.

The experiments were performed at a Bragg angle, θ_B, of 14.3° corresponding to a diffracted beam energy of 8 keV from the (111) planes. Calculations indicate that between 80 and 90 percent of the incident power was absorbed in the volume of the crystal between the diffracting surface and the coolant

channels. All data were collected with two ion chambers in the diffracted beam. By placing 0.125 inches of Al between the two chambers, rocking curves at 8 keV from the (111) planes and at 24 keV from the (333) planes were collected simultaneously in the first and second detectors, I_0 and I_1, respectively. A "cold beam" rocking curve was measured for each crystal by reducing the beam width to about 5 mm and inserting a 25-mm-thick C filter between the source and the crystal. Under "cold beam" conditions, the measured 24 keV, Si(333) rocking curve was 1.9 arcsec for the unenhanced crystal and 2.4 arcsec for the enhanced crystal.

Figure 2a and 2b shows several rocking curve scans at different power levels taken with the unenhanced crystal for the Si(111) reflection at 8 keV and the Si(333) reflection at 24 keV, respectively. Figure 3a and 3b shows similar rocking curves collected with the porous-media-enhanced crystal. The theoretical width of the Si(111) rocking curve is 10.1 arcsec FWHM and 0.6 arcsec for the Si(333) reflection. To within experimental error, less than 1 arcsec of thermal broadening occurs for the unenhanced crystal up to 601 W and no systematic broadening was observed for the enhanced crystal up to 1803 W. A summary of the rocking curve measurements is given in Table I.

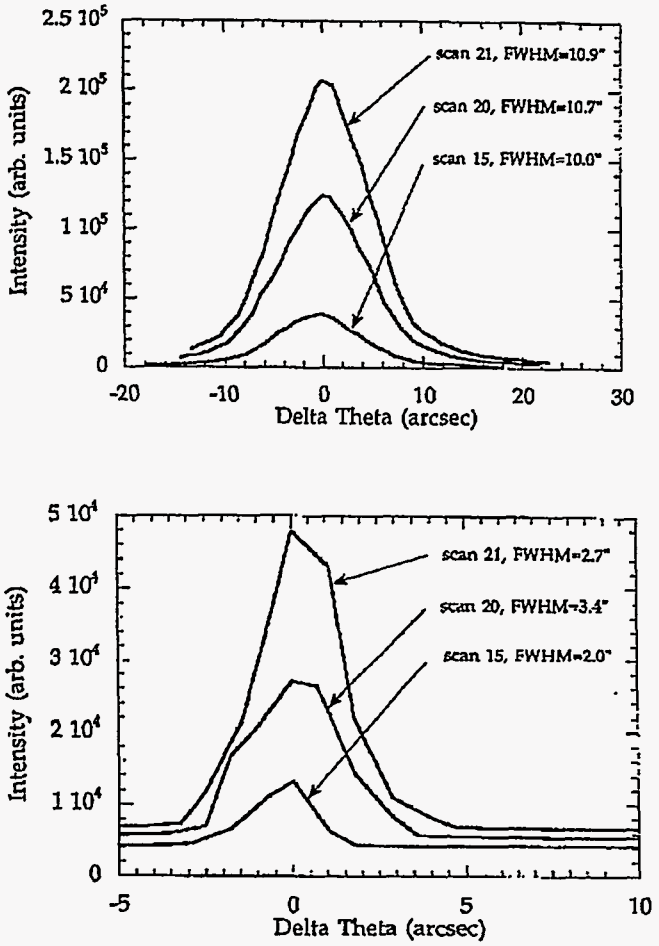

FIG. 2. Data collected with the unenhanced, smooth bore crystal. Plotted in (a) are the 8 keV rocking curves for the Si (111) reflection collected in the first ion chamber, I_0, and in (b) the 24 keV rocking curves for the Si (333) reflection collected in the second ion chamber, I_1. The peaks of the rocking curves are arbitrarily place at zero on the angle axis. The increasing intensity is due to the increasing beam size.

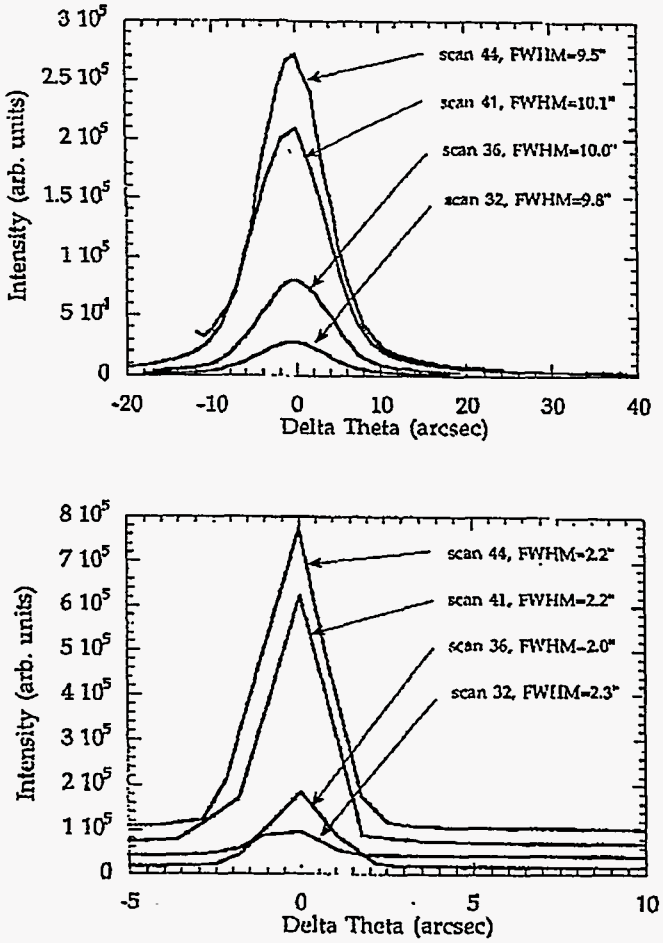

FIG. 3. Data collected with the Cu-mesh-enhanced crystal. Plotted in (a) are the 8 keV rocking curves for the Si (111) reflection collected in the first ion chamber, I_0, and in (b) the 24 keV rocking curves for the Si (333) reflection collected in the second ion chamber, I_1. The peaks of the rocking curves are arbitrarily place at zero on the angle axis. The increasing intensity is due to the increasing beam size.

When the horizontal slits were opened beyond 30 mm with the enhanced crystal for the given experimental parameters, large variations in the density of the liquid nitrogen were measured using a coriolis flow meter located downstream of the crystal. This indicated that boiling of the liquid nitrogen was probably occurring in the crystal, and no attempts were made to further increase the power. In fact, the flow rate very rapidly dropped to zero indicating that the cooling channels were "vapor-locked". Due to the fin effect and turbulent mixing in the Cu mesh insert, the fluid temperature gradient from the wall to the channel core is very shallow leading to a rapid transition from single-phase flow to saturated nucleate boiling. This results in significant generation of vapor as opposed to subcooled nucleate boiling where the bubbles detach from the wall and collapse back to

Table I. Summary of rocking curve measurements for the unenhanced and enhanced crystals.

Scan no.	Horizontal beam size (mm)	Incident power (W)	FWHM 8 keV (arcsec)	FWHM 24 keV (arcsec)	Nitrogen flow rate (l/min)	Beam current (mA)
Unenhanced						
15	4	131[a]	10.0	2.0	9.4	114.5
20	13	404[a]	10.7	3.6	10.4	108.7
21	20	601	10.9	2.7	10.4	105
Enhanced						
32	5	251[a]	9.8	2.3	10.4	108.4
36	10	596[a]	10.0	2.0	10.4	128.7
41	30	1244	10.1	2.2	13.1	89.5
44	30	1803	9.5	2.2	11.9	129.7

[a]The beam power was not measured for these scan. The power was estimated by linear extrapolation using the horizontal beam size and the measured power from scans 21, 41, and 44.

the liquid state in the subcooled core of the channel. In essence, the subcooled nucleate boiling regime is abbreviated because the core liquid temperature rises toward the saturation temperature at nearly the same rate as the liquid near the channel wall. The saturated nucleate boiling limit was primarily due to the low system pressure at which the pumping system operated because of vacuum difficulties. At higher fluid pressures, a small leak occurred at the liquid nitrogen manifold causing the pressure to rise in the vacuum chamber. Larger heat loads should be achievable at higher system pressures.

IV. FINITE ELEMENT CALCULATIONS

A detailed finite element analysis was performed for each crystal. From symmetry, only one half of the crystal was modeled. The incident power distribution was calculated and treated as being uniformly absorbed in the top 1 mm of the crystal. In the analysis, all of the incident power was assumed to be absorbed so the analysis is quite conservative. Temperature dependent material properties were used in calculating the crystal temperature profile and strain field. The thermal strain was calculated using unconstrained surface boundary conditions. A computer program was used to calculate the rocking curves from the resultant strain field using the theory of dynamical diffraction for perfect crystals.[23] The reflectivity was calculated for the distorted crystal using the average strain profile from the finite element calculations. The variation in the lattice spacing was not accounted for in the analysis. The rocking curve is the convolution of the distorted crystal and theoretical reflectivity profiles. In the model for the unenhanced crystal, the power was varied while keeping the beam cross section constant at the value used in scan 21, namely, 20 mm wide and full vertical height. This would be equivalent to changing the current in the storage ring. For the enhanced crystal, the power was varied by increasing the size of the beam cross section while keeping the current constant, equivalent to opening the slits, which is what was done experimentally. Although these two models are directly compared, it should be remembered that, in the unenhanced crystal case, the total power and power density were varied with the cross section held fixed; while for the enhanced crystal model, the power distribution, total power, and cross section were varied.

A. Unenhanced crystal

The unenhanced crystal was modeled for absorbed powers of 670 W, 1200 W, 1700 W, and 2000 W. The horizontal width of the beam was 20 mm, and the full vertical extent was accepted for all cases. Because it was not possible to know exactly what portion of the horizontal swath of radiation was accepted, a 20-mm-wide section was chosen so that the integrated power approximated the measured power from scan 21.

To incorporate boiling heat transfer into the model, a correlation was used to determine the composite forced-convection, single-phase and subcooled nucleate boiling heat flux. Following Kutateladze,[24] the superposition of the single and two-phase, forced-convection heat flux can be approximated by,

$$q'' = q''_{fc}\sqrt{1+\left(\frac{q''_{pb}}{q''_{fc}}\right)^2}, \qquad (1)$$

where q''_{fc} is the single-phase, forced-convection component and q''_{pb} is the heat flux due to pool boiling. The pool-boiling heat flux correlation used for this analysis is from Rohsenow,[25]

$$q''_{pb} = \frac{\mu_l}{i_{lg}{}^2}\sqrt{\frac{g(\rho_l-\rho_g)}{\sigma}}\left(\frac{c_{pl}\Delta T_{sat}}{C_{sf}\,\mathrm{Pr}^{1.7}}\right)^3, \qquad (2)$$

where μ_l is the liquid dynamic viscosity, i_{lg} is the heat of vaporization, g is the acceleration due to gravity, ρ_l is the liquid density, ρ_g is the vapor density, σ is the surface tension, c_{pl} is the liquid specific heat at constant pressure, Pr is the Prandtl number, and ΔT_{sat} is the wall superheat defined as the temperature difference between the wall and the saturation temperature of the liquid. The factor C_{sf} must be determined experimentally. It depends strongly on the nature

of the surface and flow geometry. In the literature for many types of conditions and fluids, C_{sf} varies from about 0.0027 to 0.015. The value used in the simulations, 0.0065, was that measured by Usui et al.,[8] for subcooled, forced-convection boiling of liquid nitrogen on a Si surface. The calculated heat transfer coefficient and heat flux as a function of wall superheat for both the unenhanced and enhanced crystals are shown in Fig. 4. In the model, the heat transfer coefficient is calculated for each interface element. Therefore, some elements may experience subcooled, forced-convection boiling and others only single-phase convection. The heat transfer correlation does not include the film boiling regime due to the uncertainty in the value of the critical heat flux. This region of uncertainty is indicated by the dashed line. It is notable that the heat transfer coefficient for the enhanced crystal is superior to the boiling heat transfer up to wall superheats of 5 K. The thermal results of the finite element analyses for the unenhanced and enhanced crystals are summarized in Table II.

Figure 5 shows the calculated temperature contours for the unenhanced (top) and enhanced (bottom) crystals for an absorbed power of 670 W. The beam cross section was 5 x 20 mm^2 in both cases. For the unenhanced crystal, the wall superheat for all channels is between about 4 and 6 K under the hottest part of the beam. For liquid nitrogen, the onset of nucleate boiling usually occurs at wall superheats of about 2 to 3 K, therefore, boiling heat transfer is beginning to dominate over single-phase forced convection in our model at this power level. The peak temperature for the unenhanced crystal is about 15.5 K higher than that for the enhanced crystal. The temperatures and gradients are smaller in the enhanced crystal because all of the channels have a very large effective heat transfer coefficient, whereas the unenhanced crystal may have a large boiling heat transfer coefficient under the hottest part of the beam but a small single-phase heat transfer coefficient in the outer channels.

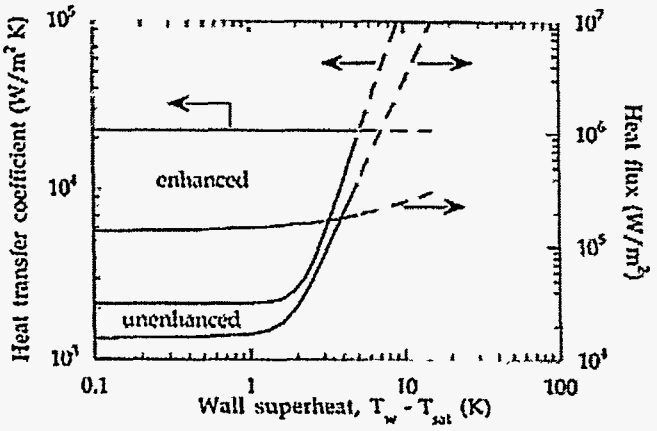

FIG. 4. Calculated heat transfer coefficient and heat flux for the enhanced and unenhanced crystals as a function of the wall superheat. The liquid properties are evaluated at saturation conditions for a pressure of 50 psi and the flow rate was 11.9 l/min.

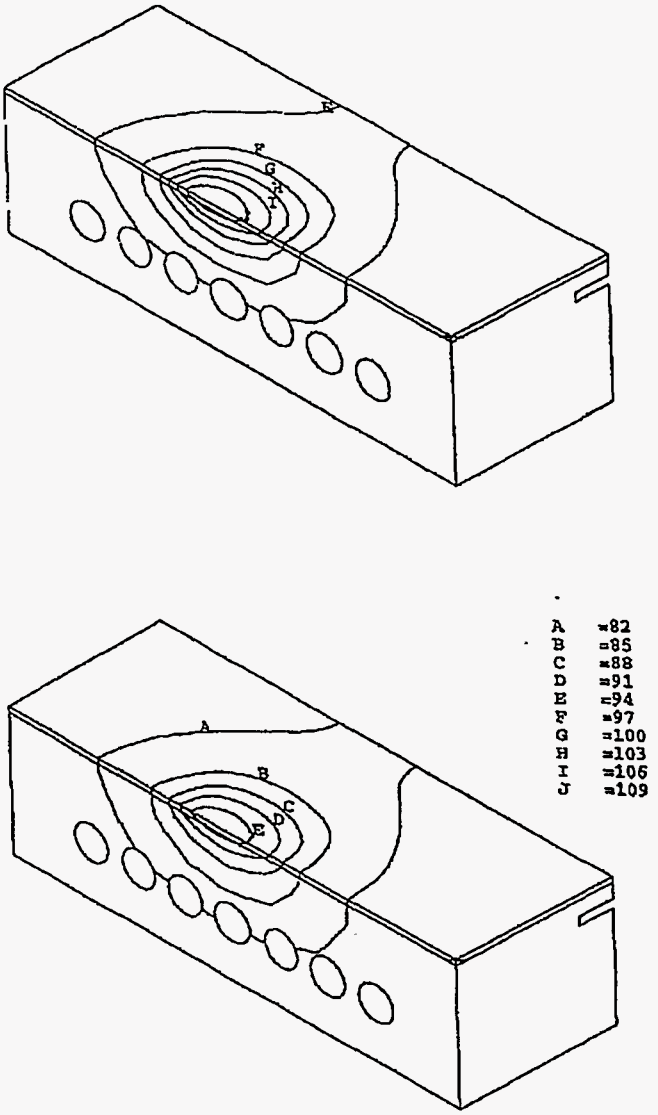

FIG. 5. Calculated temperature profile in degrees Kelvin from the finite element analysis for the unenhanced crystal (top) and the enhanced crystal (bottom). The absorbed power was 670 W, and the beam cross section was 5 x 20 mm^2. The liquid nitrogen flow rate was 11.9 l/min., and the bulk fluid temperature was 78 K.

Given the calculated value of ΔT_{sat} for the unenhanced crystal at 670 W, it can be seen from Fig. 4 that the heat flux under much of the beam footprint is between 80 and 600 kW/m^2. Usui et al.,[8] measured typical subcooled, forced-convection boiling critical heat fluxes of between 200 and 500 kW/m^2 K at comparable pressures and flow rates. Therefore, it is reasonable to assume that the experiments up to 601 W were performed below the critical heat flux condition. However, at a power level of 2000 W, the calculations indicate that the maximum wall superheat would be in excess of 9 K. This corresponds to a maximum heat flux approaching 2000 kW/m^2, which is well beyond the expected region of nucleate boiling. This raises concerns about the validity of the finite element model at power levels much greater than about 1 kW since the film boiling heat transfer regime was not included in the model. In reality

Table II. Summary of results from the finite element analysis for the unenhanced and enhanced crystals for several absorbed powers where T_{min} and T_{max} are the minimum and maximum crystal temperature, $T_{w,max}$ is the maximum channel wall temperature, and $\Delta T_{sat,max}$ is the maximum wall superheat.

Power (W)	T_{min} (K)	T_{max} (K)	$T_{w,max}$ (K)	$\Delta T_{sat,max}$ (K)
Unenhanced				
670	92.7	111.4	95.6	5.6
1200	93.1	130.4	97.5	7.5
1700	93.4	154.6	98.8	8.8
2000	93.5	173.9	99.4	9.4
Enhanced				
670	80.8	95.9	84.4	N/A
1947	87.2	132.1	97.5	N/A
2660	90.11	138.0	101.8	N/A

though, one would expect that, as film boiling develops under the hottest part of the beam, which causes the local heat transfer coefficient to drop dramatically, the heat would spread out radially and activate more nucleate boiling sites in the cooler parts of the crystal, thereby, reducing the heat flux at the center of the crystal and limiting the development of the film boiling region. Because of the high thermal conductivity of Si, the lateral spread of heat can be very significant delaying the critical heat flux to much higher power loads.

B. Porous Cu mesh enhanced crystal

A correlation for the single-phase, forced-convection heat transfer coefficient in these porous matrices has been previously reported.[14] The heat exchanger is treated as a compact matrix of wire-pin fins. The product of the effective heat transfer coefficient and surface area is given by,

$$(hA)_{eff} = \frac{h_w \eta_f A_H}{3\beta}\left(\frac{1-e^{-\beta N_{tu}}}{N_{tu}}\right), \qquad (3)$$

where h_w is the heat transfer coefficient at the mesh wire-pin, η_f is the fin efficiency, A_H is total heat transfer surface area of the channel and mesh, N_{tu} is a dimensionless parameter often used in heat exchanger analysis, and β is a correction factor derived from an energy balance. For the modeling, the liquid nitrogen was at a pressure of 50 psig and entered the crystal at 78 K. The saturation temperature was 90 K and the flow rate was 11.9 l/min. The heat transfer coefficient enhancement was calculated to be 8.84. The smooth-bore heat transfer coefficient was 2559 W/m^2 K, and the effective heat transfer coefficient of the enhanced heat exchanger was 22,621 W/m^2 K. The enhancement using liquid nitrogen was due largely to the higher efficiency of the mesh at cryogenic temperature. Because the conductivity of Cu at liquid nitrogen temperature is about 40 percent larger than at room temperature, more heat is conducted to the inner core of the channel, thereby, utilizing a greater volume of the heat exchanger.

It has been assumed that the mesh suppresses the onset of nucleate boiling (ONB) up to a maximum wall temperature of about 102 K, the value corresponding to a power of 2660 W. However, the experimental data indicated that ONB was reached for a beam power just above 1800 W. When the beam width was increased after scan 44, the flow rate dropped rapidly indicating that saturated nucleate boiling was probably occurring. It is not clear at what wall temperature boiling will occur and, therefore, render the model inconsistent since provisions for two-phase heat transfer were not included in the enhanced crystal calculations.

The results of the finite element calculations and the measured data are plotted in Figs. 6 and 7. Figure 6 shows the calculated and measured rocking curve widths as a function of power for the Si(111) reflection at 8 keV. Figure 7 shows the calculated and measured data for the Si(333) reflection at 24 keV. The measured data is plotted as a function of incident power, whereas the calculations assume complete absorption.

There is only one data point for the unenhanced crystal at which the power was measured, namely the 601 W case (scan 21). The calculations show that for the unenhanced crystal there should be no broadening up to about 700 W, after which the width of the rocking curve begins to increase rapidly. From Fig. 6, the calculations show that a 1 arcsec thermal broadening of the Si(111), 8 keV rocking curve would occur at about 1400 W. However, as pointed out earlier, the validity of the thermal calculations at this power level should be examined carefully since CHF phenomena were not included in the model. The measured data for the enhanced crystal extend to about 1800 W. At this power, the calculations give a thermal broadening of about 2.5 arcsec of the Si(333) rocking curve and the measured broadening was about 1.5 arcsec.

It is noted from Fig. 7 that the thermal broadening of the unenhanced crystal is actually slightly smaller than that of the enhanced crystal up to about 1 kW. This may be due to the fact that the coefficient of thermal expansion goes through zero and becomes negative at 125 K. At 670 W, the maximum temperature of the unenhanced crystal is 111.4 K and is 95.9 K for the enhanced crystal. Consequently, the

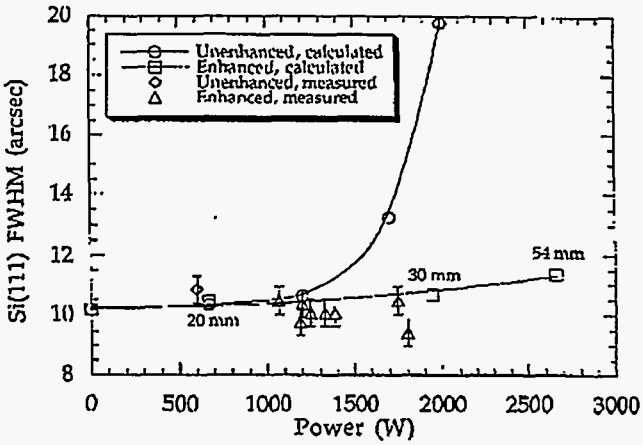

FIG. 6. Measured and calculated rocking curve widths (FWHM) for Si(111) at 8 keV for the unenhanced and enhanced crystals as a function of power. The calculated results are for absorbed power, and the measured data is for incident power. The crystals absorbed between 80 and 90 percent of the incident power.

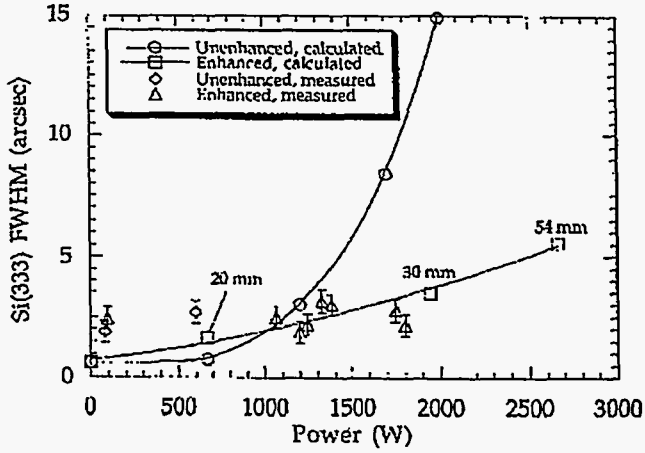

FIG. 7. Measured and calculated rocking curve widths (FWHM) for Si(333) at 24 keV for the unenhanced and enhanced crystals as a function of power. The calculated results are for absorbed power, and the measured data is for incident power. The crystals absorbed between 80 and 90 percent of the incident power.

unenhanced crystal has a smaller negative expansion coefficient and, therefore, smaller slope error than the enhanced crystal. As the power is increased above 1 kW, the expansion coefficient for the unenhanced crystal becomes positive and its magnitude is larger than that of the enhanced crystal resulting in a larger slope error.

V. SUMMARY AND CONCLUSIONS

The experimental data and the simulations indicate that a cryogenically cooled Si crystal with simple cooling channels should perform well up to at least 600 W. Some vibrations in the diffracted beam were observed, but the source of the vibrations has not been determined. With the porous media enhancement, the same crystal geometry was shown to operate well to at least 1.8 kW. Indications of boiling in the unenhanced crystal were observed at slightly above the 600 W level, but power was not increased to observe the predicted broadening of the rocking curves. Therefore, although there seems to be no conflict between the modeling and the experimental results, it is not possible at this time to say that the experiments confirm our quantitative predictions for the performance enhancement of the copper mesh crystal over the entire modeled power range. Nonetheless, these experiments have shown that the higher heat transfer coefficients achieved with the porous media inserts have a large impact on the thermal broadening at cryogenic temperatures.

Because of the improvement in the thermal conductivity of silicon at cryogenic temperatures and the relatively poor heat transfer properties of single-phase liquid nitrogen, these crystals are typically convection limited. The Biot number is a dimensionless parameter representing the ratio of the conduction to convection thermal resistance. The maximum temperature difference in the monochromator drops rapidly as the Biot number approaches unity. For the present crystal, this occurs at a heat transfer coefficient of about 70 kW/m^2 K a value almost 30 times higher than that achieved in the unenhanced crystal for single-phase forced convection. However, a Biot number of about 3 is achieved for the enhanced crystal at a flow rate of 12 l/min.

Even with beamsizes on the crystal surface as large as 20 x 30 mm^2, the measured 24 keV rocking curves were only about 2 arcsec larger than the theoretical value. This indicates that the level of strain caused by the fabrication and mounting processes is very small and spatially uniform even over a large area. These results are much better than what has been achieved with many bonded crystals for the same illuminated area. The reasons for this improved level of perfection are due to several factors all of which are indirectly related to the use of liquid nitrogen as the coolant. Because of the much higher thermal conductivity of Si at liquid nitrogen temperature, the coolant channels can be located much further from the diffraction surface. The propagation of any residual strain from the cutting of the channels, coolant pressure, or caused by the seal force is limited. Probably most important, the cryogenic crystal can be fabricated from a single block of Si. For room-temperature monochromators, the cooling channels must be as close to the diffraction surface as possible due to the smaller thermal conductivity. Consequently, a room-temperature crystal is often made from two pieces. A thin face-plate is fabricated with narrow cooling slots and then is bonded to a thicker coolant distribution base plate. No adequate bonding technique has been found to date that produces a leak-tight, radiation-hard, strain-free bond, and thus the elimination of bonding is an added bonus to the other benefits of cryogenic cooling.

ACKNOWLEDGMENTS

The authors would like to thank the staff at CHESS for their assistance in this experiment. This work is supported

by the U.S. Department of Energy, BES-Materials Sciences, under contract No. W-31-109-ENG-38.

[1]R. J. Dejus, B. Lai, E. R. Moog, and E. Gluskin, Argonne National Laboratory Report, ANL/APS/TB-17, (1994).
[2]B. Lai, A. Khounsary, and E. Gluskin, Argonne National Laboratory Report, ANL/APS/TB-11, (1993).
[3]S. Joksch, G. Marot, A. Freund, and M. Krisch, Nucl. Instrum. and Meth. in Phy. Res. **A306**, 386, (1991).
[4]G. Marot, M. Rossat, A. Freund, S. Joksch, H. Kawata, L. Zhang, E. Ziegler, L. Berman, D. Chapman, J. B. Hastings, and M. Iarocci, Rev. Sci. Instrum. **63** (1), 477, (1992).
[5]F. Comin, Rev. Sci. Instrum. **66** (2), 2082, 1995.
[6]C. S. Rogers, D. M. Mills, W-K. Lee, G. S. Knapp, J. Holmberg, A. Freund, M. Wulff, M. Rossat, M. Hanfland, and H. Yamaoka, Rev. Sci. Instrum. **66** (6), 3494, (1995).
[7]W. M. Rohsenow, "Boiling." Handbook of Heat Transfer Fundamentals, Ed. W. M. Rohsenow, J. P., Hartnett, and E. N. Ganic, 2nd ed., McGraw-Hill, 1985.
[8]T. Usiu, K. Aizawa, and Y. Sano, Proc. Soc. of Photo-Optical Instrum. Eng., **1739**, 78, (1992).
[9]V. V. Karitonov, and A. A. Plakseev, Teplofizika Vysokikh Temperatur, **20**, (4), 712, (1982).
[10]V. I. Subbotin, V. V. Karitonov, and A. A. Plakseev, Teplofizika Vysokikh Temperatur, **21**, (1), 86, (1983).
[11]B. S. Petukov, V. A. Alekseev, Y. A. Zeigarnik, F. P. Ivanov, N. P. Ikryannikiv, S. A. Kovalev, E. A. Narusbek, S. L. Solov'ev, and V. K. Shikov, Teplofizika Vysokikh Temperatur, **23**, (6), 1200, (1985).
[12]Y. A. Kuz'min, and V. V. Karishonov, Teplofizika Vysokikh Temperatur, **24**, (5), 948, (1986).
[13]V. I. Subbotin, and V. V. Karitonov, Teplofizika Vysokikh Temperatur, **29**, (2), 365, (1991).
[14]T. M. Kuzay, Rev. Sci. Instrum. **63** (1), 468, (1992).
[15]C. S. Rogers, Proc. Soc. of Photo-Optical Instrum. Eng., **1997**, 237, (1993).
[16]AuSub, 4613 series, Johnson Matthey, Electronic Materials Div., San Diego, CA.
[17]F. E. Megerlin, R. W. Murphy, and A. E. Bergles, Trans. of ASME - J. of Heat Transfer, 145, (1974).
[18]T. M. Kuzay, J. T. Collins, A. M. Khounsary and G. Morales, Proc. of ASME/JSME Thermal Eng. Conf., Vol. 5, 451, (1991).
[19]P. Doing, J. White, and Q. Shen, Nucl. Instr. & Meth. in Phy. Res. A **347**, 73, (1994).
[20]W. K. Lee, A. T. Macrander, D. M. Mills, C. S. Rogers, and R. K. Smither, Nucl. Instr. & Meth. in Phy. Res. A **320**, 381, (1992).
[21]A. T. Macrander, W. K. Lee, R. K. Smither, D. M. Mills, C. S. Rogers, and A. M. Khounsary, Nucl. Instr. & Meth. in Phy. Res. A **319**, 188, (1992).
[22]R. K. Smither, W. Lee, A. Macrander, D. Mills, and S. Rogers, Rev. Sci. Instrum. **63** (2), 1746, (1991).
[23]J. Chrzas, A. M. Khounsary, D. M. Mills, and P. J. Viccaro, Nucl. Instr. & Meth. in Phy. Res. A **291**, 300, (1990).
[24]S. S. Kutateladze, Int. J. Heat Mass Transfer, **4**, 31, (1961).
[25]W. M. Rohsenow, Trans. ASME, **74**, 969, (1952).

Performance of cryogenically cooled, high-heat-load silicon crystal monochromators with porous media augmentation

C. S. Rogers, D. M. Mills, L. Assoufid, and T. Graber
Argonne National Laboratory, Advanced Photon Source
9700 South Cass Avenue, Argonne, IL 60439 USA

(Presented on 19 Oct 1995)

The performance of two Si crystal x-ray monochromators internally cooled with liquid nitrogen was tested on the F2-wiggler beamline at the Cornell High Energy Synchrotron Source (CHESS). Both crystals were (111)-oriented blocks of rectangular cross section having identical dimensions. Seven 6.4-mm-diameter coolant channels were drilled through the crystals along the beam direction. In one of the crystals, porous Cu mesh inserts were bonded into the channels to enhance the heat transfer. The channels of the second crystal were left as drilled. Symmetric, double-crystal rocking curves were recorded simultaneously for both the first and third order reflections at 8 and 24 keV. The power load on the cooled crystal was adjusted by varying the horizontal beam size using slits. The measured Si(333) rocking curve of the unenhanced crystal at 24 keV at low power was 1.9 arcsec FWHM. The theoretical width is 0.63 arcsec. The difference is due to residual fabrication and mounting strain. For a maximum incident power of 601 W and an average power density of about 10 W/mm^2, the rocking curve was 2.7 arcsec. The rocking curve for the enhanced crystal at low power was 2.4 arcsec. At a maximum incident power of 1803 W and an average power density of about 19 W/mm^2 the rocking curve width was 2.2 arcsec FWHM. The use of porous mesh augmentation is a simple, but very effective, means to improve the performance of cryogenically cooled Si monochromators exposed to high power x-ray beams.

I. INTRODUCTION

The 7-GeV Advanced Photon Source (APS) being constructed at Argonne National Laboratory is a third-generation, hard x-ray synchrotron utilizing insertion devices to produce tunable x-ray beams of unparalleled brilliance but also of unmatched power and power density. One of the major areas of research at the APS has been to develop first optical components, monochromators, and mirrors that can handle the intense power loading without reducing the brilliance of the delivered beam due to thermo-mechanical strain. This is a formidable task considering the peak heat flux from APS undulator A can be as high as 167 W/mm^2 at normal incidence 30 m from the source, a typical position for a high-heat-load monochromator.[1] Fortunately, apertures can be placed in the beam before the optical component to reduce the total power incident on the component from the emitted 5 kW from undulator A at closed-gap to less than 1 kW depending on the size of the aperture. This is permissible because most of the usable first and third harmonic photon flux is contained within a small "central cone" on the central axis of the beam, whereas the total power envelope subtends a much larger solid angle. Conversely, APS wiggler A will produce beams of larger horizontal extent and, therefore, lower peak power density, about 80 W/mm^2, but with a total emitted power of nearly 8 kW.[2] The spectral flux for wigglers is more uniformly distributed across the beam, consequently, apertures diminish the useful flux accordingly.

The use of cryogenically cooled Si for monochromators at third-generation synchrotron radiation sources has been shown to be extremely promising.[3-6] These previous applications have been confined primarily to undulator or focused wiggler beams where, although the power density at normal incidence has been as high as 420 W/mm^2, the total absorbed power was less than 200 W. In the experiment and results described here, we have explored the use of cryogenically cooled Si under much lower average power densities, on the order of 19 W/mm^2, but for an absorbed power greater than 1.5 kW. The principle concern when handling high absorbed powers is to avoid boiling in the coolant channels. A small amount of subcooled nucleate boiling is beneficial because of the very high heat transfer coefficient, but the possibility of induced vibrations in the monochromator could make this undesirable. Subcooled nucleate boiling is defined as boiling that occurs at the liquid-solid interface when the bulk liquid temperature is below the saturation temperature. Vapor bubbles formed at the wall detach and collapse back to the liquid phase in the subcooled core of the channel. This is in contrast to saturated nucleate boiling where the bulk liquid temperature equals the saturation temperature, and a net generation of vapor occurs. A detailed description of the various regimes of boiling heat transfer can be found in Ref. 7. The heat flux range for subcooled, forced-convection nucleate boiling of liquid nitrogen is rather small, extending from about 3 to 30 kW/m^2.[8] At the top of this range, a critical heat flux (CHF) situation is encountered where the highly efficient nucleate boiling transitions to film boiling, and a thin insulating layer of gas is generated between the optic and the coolant causing a large surface temperature rise.

Because of its extremely high thermal conductivity, cryogencially cooled Si crystals are generally convection limited, that is, the largest resistance to heat flow occurs at the fluid boundary layer. Therefore, various methods to

